

# Effective Energy Function for Proteins in Lipid Membranes

Themis Lazaridis\*

Department of Chemistry, City College of the City University of New York, New York, New York

**ABSTRACT** A simple extension of the EEF1 energy function to heterogeneous membrane-aqueous media is proposed. The extension consists of (a) development of solvation parameters for a nonpolar phase using experimental data for the transfer of amino acid side-chains from water to cyclohexane, (b) introduction of a heterogeneous membrane-aqueous system by making the reference solvation free energy of each atom dependent on the vertical coordinate, (c) a modification of the distance-dependent dielectric model to account for reduced screening of electrostatic interactions in the membrane, and (d) an adjustment of the EEF1 aqueous model in light of recent calculations of the potential of mean force between amino acid side-chains in water. The electrostatic model is adjusted to match experimental observations for polyalanine, poly-leucine, and the glycophorin A dimer. The resulting energy function (IMM1) reproduces the preference of Trp and Tyr for the membrane interface, gives reasonable energies of insertion into or adsorption onto a membrane, and allows stable 1-ns MD simulations of the glycophorin A dimer. We find that the lowest-energy orientation of melittin in bilayers varies, depending on the thickness of the hydrocarbon layer. *Proteins* 2003;52:176–192.

© 2003 Wiley-Liss, Inc.

**Key words:** implicit solvation; molecular dynamics simulations; transmembrane helices; glycophorin A; bacteriorhodopsin; melittin; 18A

## INTRODUCTION

Of all proteins in the cell, 20–30% are associated with biological membranes, and most drug targets are membrane-associated receptors. These proteins perform a multitude of important biological functions. Elucidation of the mechanism of their action requires knowledge of their three-dimensional structure and the conformational changes they undergo. X-ray crystallography and NMR spectroscopy have been enormously successful in revealing the structure of soluble proteins, but they face formidable difficulties when applied to membrane proteins. As a result, only a handful of membrane protein structures are known at atomic resolution. Under these circumstances, computer modeling could make a significant contribution.

The most detailed and accurate approach to modeling membrane proteins involves explicit representation of the lipid and water molecules. The first molecular dynamics (MD) simulation of a lipid bilayer was published in 1988.<sup>1</sup>

Since then, many more simulations of systems of ever-increasing size and complexity have been simulated.<sup>2–4</sup> In addition to pure lipid bilayers, simulations have been carried out on proteins or peptides embedded in bilayers<sup>5</sup> (e.g., gramicidin,<sup>6</sup> bacteriorhodopsin,<sup>7</sup> melittin,<sup>8,9</sup> the OmpF trimer,<sup>10</sup> and cholesterol in a DPPC bilayer<sup>11</sup>). A study of the glycophorin A dimer in an explicit membrane gave insights into peptide-peptide and peptide-lipid interactions.<sup>12</sup>

All-atom explicit simulations provide the most realism but are computationally expensive. In addition, they do not easily provide information on the thermodynamics of the insertion or folding process because free energies are obtained only with laborious procedures. An alternative approach is continuum electrostatics, which provides the electrostatic component of the free energy with modest computational expense. Such calculations were used to study the energetics of insertion into lipid bilayers of polyalanine,<sup>13</sup> alamethicin,<sup>14</sup> the hemagglutinin fusion peptide,<sup>15</sup> and an anticonvulsant drug.<sup>16</sup> Predictably, they found the hydrophobic interaction to be the driving force. However, they also identified a previously unrecognized opposing force: the desolvation of the polar groups, even if they are involved in hydrogen bonds. They also determined the free-energy profile for the insertion process. The association of peripheral membrane proteins with membranes<sup>8,17,18</sup> and the permeation of ions through ion channels<sup>19</sup> have also been studied with the Poisson–Boltzmann method.

Continuum electrostatics calculations lead to large savings in computer time but have their own limitations. First, they provide only the electrostatic component of the free energies. The remainder is usually approximated by a term proportional to the solvent-accessible surface area. Calculations of accessible surface areas can slow down a simulation considerably. In addition, performing MD simulations with solution of the Poisson–Boltzmann equation every step or even every certain number of steps is exceedingly slow. Therefore, more approximate, empirical

*Abbreviations:* MD, molecular dynamics; TM, transmembrane; GpA, glycophorin A TM domain; bRMSD, backbone root-mean-square deviation.

Grant sponsor: National Science Foundation; Grant number: DBI-9974621.

\*Correspondence to: Themis Lazaridis, Department of Chemistry, City College of the City University of New York, 138th St. & Convent Ave., New York, NY 10031. E-mail: themis@sci.cuny.cuny.edu

Received 29 September 2002; Accepted 17 December 2002

models have been pursued where the membrane is treated as a slab of a continuous medium with lipid-like properties embedded in another medium with water-like properties.<sup>20–27</sup> A gradual transition between the two is commonly used. Most models are based on experimental data for the free energy of transfer of amino acids from water to a nonpolar phase, usually octanol, parameterized in terms of accessible surface area. Brasseur et al.<sup>21</sup> performed conformational analysis of an ionophore at an implicit membrane interface across which the dielectric constant varied from 3 to 30. Jahnig and Edholm<sup>23</sup> performed simulations of bacteriorhodopsin in the presence of a hydrophobic potential applied to exposed atoms parameterized based on octanol-water transfer free energies but without adjusting the electrostatic interactions. Similar terms were used as restraints in another modeling approach.<sup>20</sup> Other groups conducted conformational analyses of glycolipids at an implicit membrane interface with a transfer free energy term and adjustment of the dielectric constant.<sup>24,25</sup> Milik and Skolnick performed Monte Carlo simulations of peptide insertion into membranes on<sup>28</sup> and off<sup>26</sup> a lattice. They used a simplified polypeptide chain representation (C $\alpha$  atoms only) and a schematic energy function. As a result, their model is applicable only to short monomeric, helix-forming peptides. Extensions of this type of work have been published more recently.<sup>29–31</sup> Efremov and coworkers<sup>27,32,33</sup> developed a surface area-based implicit solvation model for a nonpolar phase and for a heterogeneous membrane-water system<sup>34</sup> and applied it to Monte Carlo simulations of hemagglutinin fusion peptide analogs<sup>35</sup> and cardiotoxins.<sup>36</sup> The “dipole potential” of a membrane, due to the nonuniformity of charge distribution in the headgroup region of a zwitterionic lipid bilayer, was also calculated and incorporated in implicit membrane models.<sup>37</sup> In a different type of model, the protein is embedded in a lattice of Langevin dipoles.<sup>38</sup> The membrane is modeled by making the dipole moments of the dipoles inside the membrane smaller than those of the dipoles outside the membrane. These dipole moments and an additional scaling parameter are adjusted to reproduce the solvation free energies of small molecules in water and nonpolar media. This model is not really an implicit model, but rather a simplified explicit model, and, although cheaper computationally than full atomic detail simulations, it is not as efficient and convenient as implicit models.

At the other end of the spectrum of computational methods, membrane proteins are often simulated in vacuum. For example, studies of G-protein-coupled receptors were performed by using a constant dielectric<sup>39</sup> or a distance-dependent dielectric.<sup>40</sup> Some studies focused on prediction of side-chain packing in membrane proteins using a vacuum force field.<sup>41,42</sup> Brunger and coworkers<sup>43,44</sup> used simulated annealing together with mutagenesis data to predict the structure of the glycoprotein dimer. The second of these predictions<sup>44</sup> was shown to be quite close to the structure determined later by NMR.<sup>45</sup> Similar work was performed to predict a structure for the neu receptor.<sup>46</sup> Simulations in vacuum with experimental con-

straints were also successfully used to predict the structure of rhodopsin.<sup>47,48</sup> Such models turned out to be quite good when the crystal structure of this protein became available.<sup>49</sup> Because the membrane interior is nonpolar, simulations in vacuum may actually give realistic behavior for many applications. However, omission of the favorable interaction of the peptides with the lipids will lead to overestimation of their attractive forces in the bilayer. In addition, effects such as helix tilt due to hydrophobic mismatch cannot be reproduced by vacuum simulations.

Most of the above models were designed to yield the energy as a function of position and orientation with respect to a bilayer for a given peptide or protein conformation and not the effective energy of different conformations. For example, far from the membrane most of the models revert to a vacuum force field, which is clearly not appropriate for aqueous solution. Here we propose an energy function that is designed to do both. Far from the membrane the function is equivalent to EEF1, a well-tested model for aqueous solution. Like EEF1, the new function provides atomistic detail for the protein, is computationally efficient, and provides analytical energy derivatives important for energy minimization and dynamics. Therefore, it can be used to study the folding process of membrane proteins. With some further fine-tuning, this function could provide a means to obtain quantitative estimates of the free energy of binding of peptides to membranes.

## ENERGY FUNCTION

### EEF1

Our starting point is an effective energy function for soluble proteins, EEF1.<sup>50,51</sup> This function is based on the CHARMM polar hydrogen force field<sup>52</sup> and differs from it mainly in two ways: (a) an implicit solvation term that describes the “self-energy” of all atoms (the interaction of each atom with the solvent) is added and (b) the ionic side-chains are neutralized and a distance-dependent dielectric constant ( $\epsilon = r$ ) is used for the electrostatic interactions. The implicit solvation term has the form<sup>50,51</sup>:

$$\Delta G_i^{\text{solv}} = \sum_i \Delta G_i^{\text{solv}} = \sum_i \Delta G_i^{\text{ref}} - \sum_{i \neq j} f_i(r_{ij}) V_j \quad (1)$$

where  $\Delta G_i^{\text{solv}}$  is the solvation free energy of atom  $i$ , and  $r_{ij}$  is the distance between  $i$  and  $j$ . Eq. 1 says that the solvation free energy of atom  $i$  is that in a small model system where the atom is fully exposed to solvent ( $\Delta G_i^{\text{ref}}$ ) minus the solvation free energy it loses due to the presence of surrounding atoms. The solvation free energy density is modeled as a Gaussian function

$$f_i(r) 4\pi r^2 = \alpha_i \exp(-x_i^2), \quad x_i = \frac{r - R_i}{\lambda_i} \quad (2)$$

where  $R_i$  is the van der Waals radius of  $i$  (one half the distance to the energy minimum in the Lennard-Jones potential),  $\lambda_i$  is a correlation length (3.5 Å for most atoms), and  $\alpha_i$  is a proportionality coefficient given by

$$\alpha_i = 2\Delta G_i^{\text{free}} / \sqrt{\pi} \lambda_i \quad (3)$$

**TABLE I. Transfer Free Energies From Vapor Phase to Cyclohexane (kcal/mol)**

	Exper <sup>a</sup>	Groups	Calc by group additivity
Leu	-2.64	3 CH3E + 1 CH1E	-2.64
Ile	-2.77	2 CH3E + 2 CH2E	-2.77
Val	-2.05	2 CH3E + 1 CH2E	-2.05
Met	-3.83	2 CH3E + CH2E + S	-3.83
Cys	-2.52	CH3E + SH1E	-2.52
Phe	-3.74	CH3E + CR + 5 CR1E	-4.06
Trp	-8.21	CH3E + 3 CR + 5 CR1E + NH1	-7.91
Tyr	-5.97	CH3E + 2 CR + 4 CR1E + OH1	-5.97
Thr	-2.31	CH3E + CH2E + OH1	-2.34
Ser	-1.66	CH3E + OH1	-1.63
His	-5.61	CH3E + CR + 2 CR1E + NR + NH1	-5.61
Gln	-3.84	CH3E + CH2E + CO + NH2	-3.80
Asn	-3.04	CH3E + CO + NH2	-3.08
Lys	-3.97	CH3E + 3 CH2E + NH3	-3.97
Glu	-3.43	CH3E + CH2E + 2 OC	-3.18
Asp	-2.23	CH3E + 2 OC	-2.46
Arg	-5.00	CH3E + 2 CH2E + CR + NH1 + 2 NC2	-5.00

<sup>a</sup>Ref. 63. Ala (CH<sub>3</sub>) and Gly (H<sub>2</sub>) were omitted. For the titratable molecules, the data refer to the neutral form. The atom types are as follows: CR: carbon with no hydrogens; CR1E: extended aromatic carbon with 1 H; CH1E: extended aliphatic carbon with 1 H; CH2E: extended aliphatic carbon with 2 H; CH3E: extended aliphatic carbon with 3 H; NH1: amide nitrogen; NR: aromatic nitrogen with no hydrogens; NH2: nitrogen bound to two hydrogens; NH3: nitrogen bound to three hydrogens; NC2: guanidinium nitrogen; N: proline nitrogen; OH1: hydroxyl oxygen; O: carbonyl oxygen; OC: carboxyl oxygen; S: sulfur; SH1E: extended sulfur with one hydrogen.

where  $\Delta G_i^{\text{free}}$  is the solvation free energy of the free (isolated) atom  $i$ ;  $\Delta G_i^{\text{free}}$  is close but not identical to  $\Delta G_i^{\text{ref}}$  and is determined by requiring that the solvation free energy of deeply buried atoms be zero. The above solvation model (Eq. 1) was added to the CHARMM force field to obtain an approximation for the effective energy of the protein,

$$W_{\text{EEF1}} = E + \Delta G^{\text{slv}} \quad (4)$$

EEF1 has been tested extensively.<sup>51</sup> It gives modest deviations from crystal structures upon molecular dynamics simulations at room temperature, unfolding pathways in agreement with explicit solvent simulations, and it discriminates native conformations from misfolded decoys.<sup>53</sup> It has been used to determine the folding free energy landscape of a  $\beta$ -hairpin,<sup>54</sup> exploration of partially unfolded states of  $\alpha$ -lactalbumin,<sup>55</sup> studies of protein unfolding,<sup>50,56–58</sup> identification of stable building blocks in proteins,<sup>59</sup> and analysis of the energy landscape of polyalanine.<sup>60</sup>

Recent calculations of the potential of mean force between ionizable side-chains in water<sup>61</sup> showed, however, that EEF1 overestimates the attraction between unlike charged and hydrogen bonding groups. In addition, as was originally reported,<sup>51</sup> certain interactions involving arginine were not correct. This work is based on a modified set of partial charges for the ionizable and polar side-chains designed to optimize the agreement with the calculated potentials of mean force (see Appendix). This new version of the energy function is referred to as EEF1.1, and its extension to membranes presented below is referred to as IMM1 (Implicit Membrane Model 1).

### Solvation Parameters for the Nonpolar Core of Lipid Bilayers

For molecules immersed in a membrane, the values  $\Delta G_i^{\text{ref}}$  must correspond to a nonaqueous phase. Because data for the solvation free energy of molecules in the hydrocarbon core of membrane are not available, we had to use data for a model nonpolar solvent. A common choice for this purpose is octanol.<sup>62</sup> However, octanol has hydrogen-bonding potential and dissolves significant amounts of water.<sup>63</sup> Therefore, we chose to use data for the distribution of amino acid side-chain analogs between cyclohexane and the gas phase.<sup>63</sup> The data used (in Ben-Naim's standard state<sup>64</sup>) are shown in Table I.

To extract atomic contributions to the solvation free energy (the  $\Delta G_i^{\text{ref}}$  values), we used the following procedure. First, the data for Leu, Ile, and Val were used to derive parameters for CH3E, CH2E, and CH1E. The resulting group contributions (Table II) are similar to those that can be derived from data for the solvation of alkanes or alkenes in their neat liquids.<sup>64</sup> These data also show that the presence of a double bond makes a very small difference in the solvation free energy. Then, the data for Cys and Met were used to derive the values for S and SH1E, and Lys was used to extract a value for NH3/NH2 (the experimental data are for the neutral form of the ionizable residues). Then, the Gln and Asn data were used to extract an average value of 1.27 kcal/mol for CO. The remaining data show significant nonadditivity, which is surprising in a nonpolar solvent. For example, the OH1 in Tyr seems to make a much larger contribution than in Ser and Thr, and the solvation free energy of the acids is smaller than one would expect from their composition. Blind fitting of the

**TABLE II. Atomic Contribution to the Solvation Free Energy in Water and Cyclohexane**

	Water	Chex		Water	Chex
CR	-0.890	-1.350	NH3	-20.000	-1.145
CH1E	-0.187	-0.645	NC2	-10.000	-0.200
CH2E	0.372	-0.720	N	-1.000	-1.145
CH3E	1.089	-0.665	OH1	-5.920	-0.960
CR1E	0.057	-0.410	O	-5.330	-1.270
NH1	-5.950	-1.145	OC	-10.000	-0.900
NR	-3.820	-1.630	S	-3.240	-1.780
NH2	-5.450	-1.145	SH1E	-2.050	-1.855

remaining data using singular value decomposition<sup>65</sup> gives zero contribution to NC2 and a large difference between CR and CR1E. As a compromise, we set the value for NC2 = -0.2 and the value for NH1 the same as NH2 and obtained the atomic contributions shown in Table II together with those in water. The transfer free energies calculated by using these group contributions are shown in the last column of Table I. Because the number of unknown parameters is almost as large as the number of data points, the data are fit well. The large difference between CR and CR1E or the very small value for NC2 is a bit unsettling. Nevertheless, the most important parameters, those for the nonpolar groups and the peptide backbone, seem reasonable.

The solvation free energy of nonpolar groups is small positive in water and small negative in cyclohexane. Polar groups have negative solvation free energies in both solvents but of larger magnitude in water. Therefore, as expected, transfer of nonpolar groups to the lipids is favorable, whereas transfer of polar groups is unfavorable. The  $\Delta G_i^{\text{free}}$  values in cyclohexane are obtained by using the same ratio of  $\Delta G_i^{\text{free}}/\Delta G_i^{\text{ref}}$  as in water.

Monovalent charged groups have a solvation free energy in water of about -80 kcal/mol. Burial of a charged group in a membrane in the absence of favorable interactions does not cost -80 kcal/mol because neutralization of the group and burial of the neutral group cost much less energy. Neutralization costs

$$\pm 2.3 \text{ RT}(\text{pK} - \text{pH}) \quad (5)$$

which is 1–8 kcal/mol, depending on the pK and the pH. Burial of the neutral group costs up to 10 kcal/mol. Therefore, the total cost is 10–20 kcal/mol. The charged groups in EEF1 do not carry a net charge and have a lower solvation free energy ( $\Delta G_i^{\text{ref}}$  values of EEF1 in Table II). Thus, conveniently, the burial of charged groups in this model gives free energy costs of the right order of magnitude, although explicit use of Eq. 5 is required for more accurate results.

### Modeling the Membrane

Next we introduce the following model for the membrane, considered to be parallel to the xy plane with its center at  $z = 0$ . The solvation parameters of all atoms ( $\Delta G_i^{\text{ref}}$  and  $\Delta G_i^{\text{free}}$ ) now depend on the vertical direction,  $z$ , or  $z' = |z|/(T/2)$ , where  $T$  is the thickness of the nonpolar

core of the membrane (usually 20–30 Å, depending on the lipid<sup>66</sup>; see also <http://aqueous.labs.brocku.ca/lipid/>):

$$\Delta G_i^{\text{ref}}(z') = f(z')\Delta G_i^{\text{ref, wat}} + (1 - f(z'))\Delta G_i^{\text{ref, chex}} \quad (6)$$

The function  $f(z')$  describes the transition from one phase to the other. Most previous studies used an exp or an arctan function, but the following function is just as good:

$$f(z') = \frac{z'^n}{1 + z'^n} \quad (7)$$

where  $n$  controls the steepness of the transition. The exponent  $n = 10$  gives a region of 6 Å over which the environment goes from 90% nonpolar to 90% polar. This corresponds roughly to X-ray and neutron diffraction data for the structure of the lipid bilayers.<sup>67</sup> The midpoint of the transition ( $f = 0.5$ ) corresponds to the hydrocarbon-polar headgroup interface. Hence, as in most other hydrophobic slab models, the headgroup region is assumed to have the same properties as aqueous solution. The validity of this assumption is questionable, but there is little else we can do at this point because no data are available for the solvation free energy of different types of molecules in the headgroup region of membranes (see Discussion). When such data become available, they could be easily incorporated in the model by proper modification of the  $f(z')$  profile.

This model was applied to a number of model systems, including a polyaniline helix, bacteriorhodopsin, and glycophorin (see Tests below). In all cases it was found that the change in effective energy upon membrane insertion ( $\Delta W$ ) was unfavorable. This results from the contribution of the polar groups, which, even when they are hydrogen bonded to other groups, have a residual solvation free energy, most of which is lost when they move into the lipid environment. This is in agreement with Poisson-Boltzmann calculations.<sup>13</sup> The error lies in the fact that  $\Delta G_i^{\text{ref}}$  values deal only with the self energy of the atoms. A second effect is the effect of environment on electrostatic interactions. This issue is addressed in the following section.

### Electrostatic Interactions

To account for the strengthening of electrostatic interactions in the membrane in a way that is compatible with the distance-dependent dielectric used in EEF1, we introduce a modified dielectric screening function

$$\epsilon = r^{f_{ij}} \quad (8)$$

where  $f_{ij}$  depends on the position of the interacting atoms with respect to the membrane. Far from the membrane,  $f_{ij}$  is equal to 1 so that we recover the RDIE model. The model

$$f_{ij} = \sqrt{f_i f_j} \quad (9)$$

with  $f_i, f_j$  given by Eq. 7, which gives  $\epsilon = 1$  in the center of the membrane, seemed initially reasonable but was found to strengthen electrostatic interactions too much. Therefore, we used the empirical model

$$f_{ij} = a + (1 - a)\sqrt{f_i f_j} \quad (10)$$

**TABLE III. Insertion Energies (kcal/mol) by PB/SA and Present Model**

	(Ala) <sub>25</sub>	(Leu) <sub>25</sub>	GpA
PB/SA			
PB ( $\epsilon = 1$ )	+32	+25	+92
PB ( $\epsilon = 2$ )	+23	+18	+66
SA (nonpolar)	-38	-56	-84
PB/SA ( $\epsilon = 1$ )	-6	-31	+8
PB/SA ( $\epsilon = 2$ )	-15	-38	-18
Present model (IMM1)			
$\Delta\Delta G^{\text{solv}}$	+47	-20	+44
Aliphatic	-23	-63	-68
Aromatic			-7
Polar	+69	+43	+119
$\Delta E^{\text{elec}}$			
( $a = 0.85$ )	-36	-36	-76
( $a = 0$ )	-376	-378	-784
$\Delta W$ ( $a = 0.85$ )	+11	-56	-41

with a an adjustable parameter. The value  $a = 0.85$  was found to give reasonable results (see below).

### TESTS

In the following tests we usually report the effective energy of the final structure after MD simulation followed by 300 energy minimization steps. This protocol is rather arbitrary and, therefore, the values given would differ if one did the simulation with different initial random velocities or a different number of minimization steps. Only differences in energy between different conformations are meaningful, and these are much less affected by the protocol. In principle, what one is interested in is the free energy of a state, which is equal to the average effective energy (which includes the solvation free energy) plus the conformational entropy. Similarly, comparison with experiment should not be performed with a single structure but an ensemble of structures, especially in the case of peptides, which may not have a well-defined conformation and position. However, here we are not attempting to provide accurate free energy estimates but to make an initial assessment of the validity of the model. In some cases, we also report average effective energies over the last 5 ps of simulation.

### Transmembrane Helices: Polyalanine, Polyleucine, and Glycophorin A

The ideal (Ala)<sub>25</sub> and (Leu)<sub>25</sub> helices and the dimeric transmembrane (TM) domain from Glycophorin A (GpA) were used for initial evaluation and calibration of the model. Poisson–Boltzmann (PB/SA) calculations were also performed for comparison by using a membrane dielectric constant of either 1 or 2 and a nonpolar contribution proportional to the surface area buried in the membrane. The results are shown in Table III. The  $\epsilon = 1$  model predicts favorable energies of insertion for polyalanine and polyleucine but unfavorable energy for GpA. Because it is well established that the GpA TM does indeed insert, this model can be rejected. The  $\epsilon = 2$  model predicts favorable insertion energies for all three model systems.

The “self-energy” part of the present model (Eq. 1) gives a favorable energy only in polyleucine, where the favorable aliphatic solvation change dominates the unfavorable polar solvation change. For the other two systems, the polar contribution dominates. This finding shows that to reproduce the experiment, it is necessary to include the strengthening of electrostatic interactions in the membrane. Going from  $\epsilon = r$  in water to  $\epsilon = 1$  in the center of the membrane gives a change in electrostatic energy that is clearly too large. This led to us to adopt Eq. 10 with  $a$  as an adjustable parameter. A value for  $a$  in the range 0.8 to 0.9 gives reasonable results. We tentatively adopted the value 0.85. Data on the insertion free energy could be used in the future to make finer adjustments to this factor. With this value we obtain an unfavorable insertion energy for polyalanine and large favorable energies for polyleucine and GpA (Table III), quite different from the PB/SA results. The difference may be related to the way the hydrophobic contribution is calculated.

Experimental data for the interaction of polyalanine with bilayers are somewhat conflicting.<sup>68</sup> Moll and Thompson<sup>69</sup> reported that an (Ala)<sub>20</sub> peptide fused to BPTI bound to vesicles, in unknown orientation, with a free energy of about  $-5$  kcal/mol. Chung and Thompson<sup>70</sup> found that a different Ala-based peptide bound poorly to lipid vesicles, although replacement of just three residues by Leu led to binding in a TM orientation. More recently, an Ala-based peptide was found to have insufficient hydrophobicity to be inserted into lipid bilayers in a transbilayer orientation, whereas a Leu-based peptide did.<sup>71</sup> The tentative conclusion from these studies is that polyalanine is at best a marginal TM helix former, whereas polyleucine is definitely a good TM helix former.<sup>68,72</sup> Therefore, a positive  $\Delta W$  for polyalanine is acceptable. The fact that PB/SA ( $\epsilon = 2$ ) predicts for polyalanine an energy of insertion almost as favorable as that of GpA seems problematic for this model, given the above experimental observations.

A 200-ps MD simulation of (Ala)<sub>25</sub> starting from the TM position shows little change from the initial, TM helix. Although the TM state is higher in energy than the aqueous helix, there is a significant barrier for the transition due to the need for one terminus to cross the membrane. The interfacial position of (Ala)<sub>25</sub> (with the helical axis on the midplane and the termini oriented toward the aqueous phase) is 7 kcal/mol higher than the TM position. A 300-step energy minimization further reduces this difference to 1 kcal/mol. This is in agreement with solid-state NMR results showing that the TM position for polyalanine is only slightly more favorable than the interfacial position.<sup>68</sup> A 100-ps simulation starting from an adsorbed position leads to the peptide moving away from the membrane, showing that the interfacial local minimum is shallow. A 200-ps simulation of (Leu)<sub>25</sub> shows the helix adopting a 39° tilt with respect to the bilayer normal (Fig. 1). The tilting is caused by the need to immerse in the membrane core more hydrophobic Leu side-chains and is dependent on the thickness of the slab. A simulation with  $T = 34$  Å produces a smaller tilt (14°).

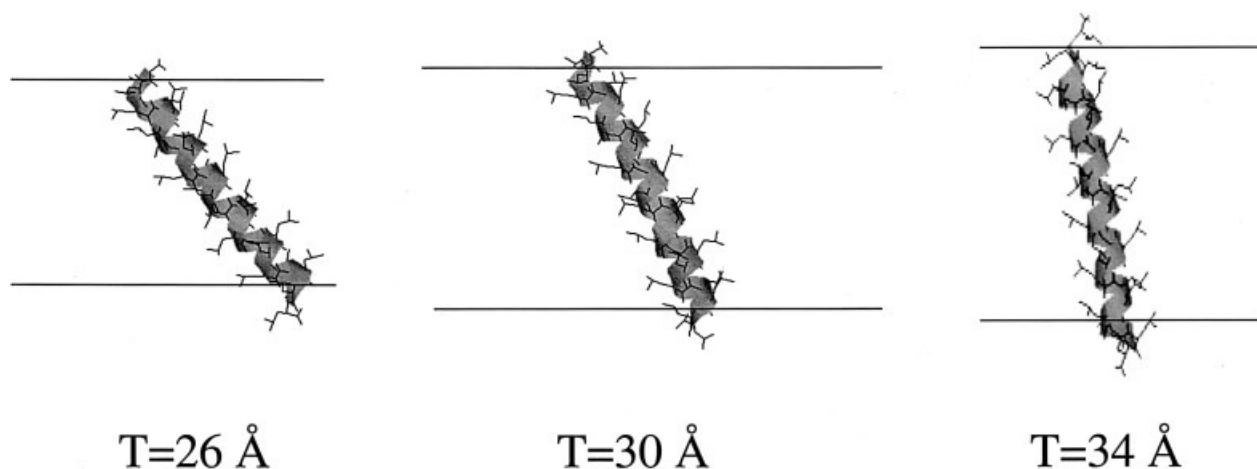


Fig. 1. Polyleucine TM helix after dynamics at different nonpolar core thicknesses. In all figures, the horizontal lines denote the hydrocarbon core-polar headgroup boundary ( $f = 0.5$ ).

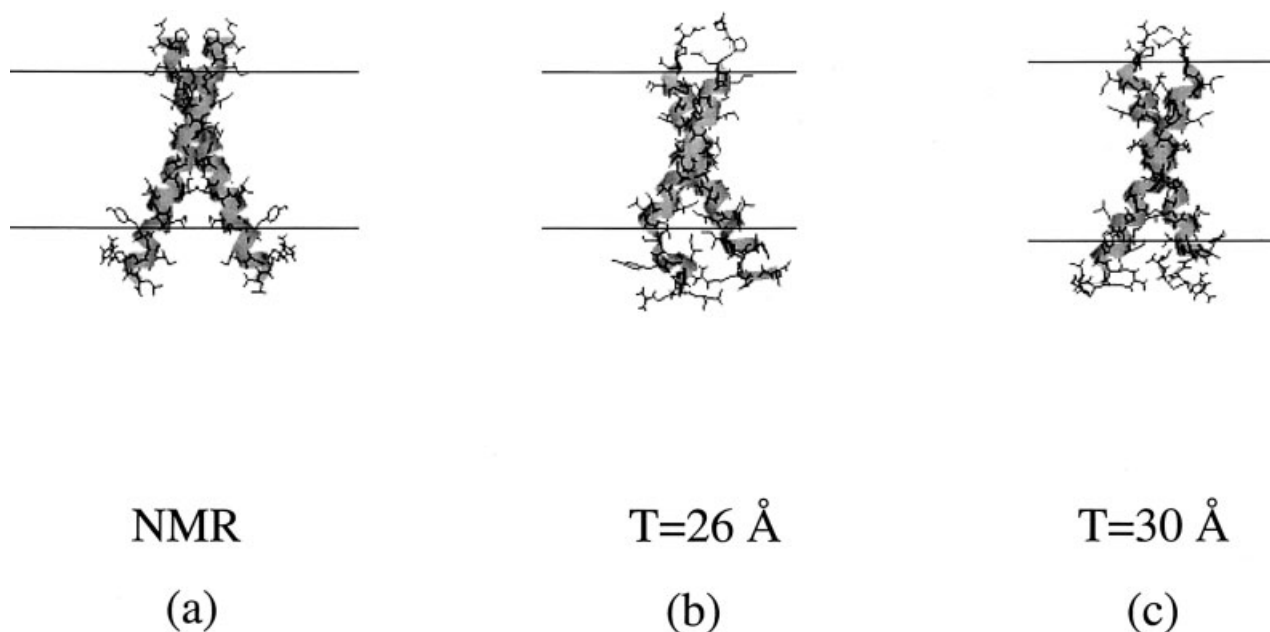


Fig. 2. Glycophorin A dimer structure from experiment and after 1-ns MD simulation at nonpolar core thickness 26 and 30 Å.

In a more stringent test, MD simulations of the GpA dimer starting from the solid-state NMR structure<sup>73,74</sup> were performed. The structure provides coordinates for residues 73–95. The flanking polar residues of the peptides used in the experiments (70–72, 96–98) were built as an ideal  $\alpha$ -helix. A 1-ns simulation gives a 1.8 Å backbone root-mean-square deviation (bRMSD) for the TM portion. The final structure from this simulation is shown in Figure 2(b). The major change is a break of one helix near the C-terminus, caused by either the interaction between the polar residues or the preference of an Ile residue to be buried in the hydrocarbon core. The same simulation with  $T = 30$  Å gives 1.4 Å bRMSD. This time one turn near the C-terminus of one helix unfolds [Fig. 2(c)]. Table IV shows the results of geometric analysis for the three structures.

The smaller tilt and crossing angles in the thicker membrane are as expected from the concept of “hydrophobic matching.” The solid-state NMR experiments<sup>74</sup> were carried out in DMPC or POPC bilayers, with hydrocarbon core thickness 23<sup>66</sup> and 27 Å,<sup>68</sup> respectively. Therefore, the  $T = 26$  Å model is closer to these experiments. It should be noted that the experiments have so far provided information on the structure near the helix crossing point. The structure outside the membrane is unknown.

The heterogeneous membrane system is necessary for maintenance of the dimer structure. A 200-ps simulation in pure implicit cyclohexane (with  $\epsilon = 1$ ) gives an 11 Å bRMSD, with the helices adopting an antiparallel orientation. A 200-ps simulation in implicit water gives 4.3 Å bRMSD with a shift of the two helices and partial loss of

**TABLE IV. Geometric Properties of the Two Helices in GpA<sup>†</sup>**

	NMR	MD T = 26 Å	MD T = 30 Å
Helix 1 tilt	(21) <sup>a</sup>	24	23
Helix 2 tilt	(21)	23	17
Crossing angle	43	46	40
Distance	6.4 Å	7.1 Å	5.9 Å
bRMSD	—	1.8 Å	1.4 Å

<sup>†</sup>Only the TM residues (73–95) are used in the analysis.

<sup>a</sup>The tilt is not known from the experiment. This value results from placing the dimer with its principal axis along the bilayer normal.

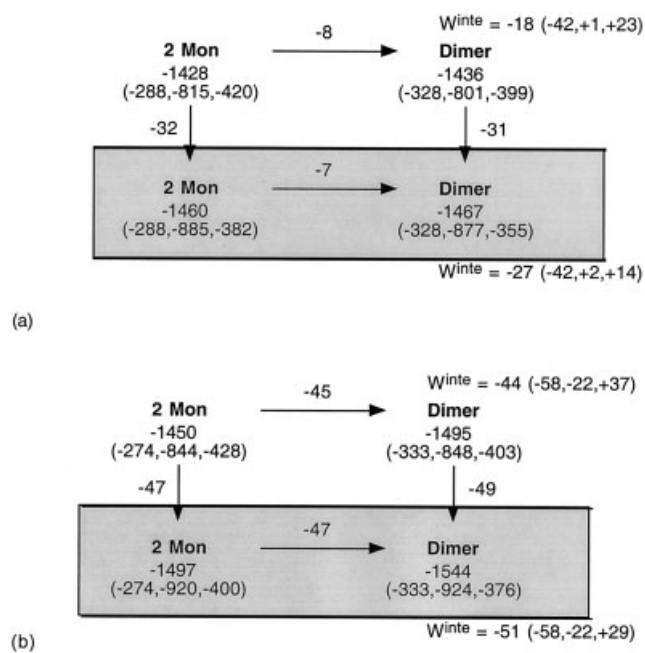


Fig. 3. Thermodynamic cycle for glycoporphin A dimer insertion and association based on (a) minimized structures (b) minimized structures after 200 ps of dynamics. All values are in kcal/mol. The numbers in parentheses are the van der Waals, electrostatic, and solvation contributions, respectively. The gray region symbolizes the membrane. The numbers over/next to arrows are the changes in effective energy for that reaction.  $W^{\text{inte}}$  is the interaction energy between the helices.

$\alpha$ -helical structure and formation of  $\pi$  bulges. A 200-ps simulation in vacuum gives 2.7 Å bRMSD with reduction of the crossing angle [simulations in vacuum do not produce large shifts for kinetic reasons (i.e., larger energy barriers between local minima)].

The complete association/insertion cycle for GpA based on minimized structures is shown in Figure 3(a). The effective energy of association is favorable in both water and membrane. The lowest energy state is the dimer in the membrane. The interaction energy between the two helices ( $W^{\text{inte}}$ ) in the dimer is larger than the association energy. This is because the dimer structure forces the helices to adopt a tilt with respect to the bilayer, and this tilting causes a solvation free energy loss for some polar residues near the boundary. Because minimization alone may not be sufficient to find the optimal location of the

**TABLE V. Energies of Trp, Tyr, and Phe Side-Chains in Different Environments (kcal/mol)**

	Core	Interface	Water
Trp			
Total W	+4.8	+3.1	+4.8
$\Delta G^{\text{solv}}$	-7.7	-9.4	-7.7
Aliphatic	-0.62	-0.42	+0.32
Aromatic	-5.97	-4.75	-2.34
Polar	-1.09	-4.20	-5.67
Tyr			
Total W	-6.35	-9.04	-7.27
$\Delta G^{\text{solv}}$	-5.76	-8.45	-6.67
Aliphatic	-0.65	-0.62	+0.34
Aromatic	-4.21	-3.23	-1.51
Polar	-0.89	-4.61	-5.50
Phe			
Total W	-4.16	-2.46	-0.44
$\Delta G^{\text{solv}}$	-4.00	-2.3	-0.28
Aliphatic	-0.65	-0.28	+0.33
Aromatic	-3.35	-2.03	-0.61

side-chains in the monomer and dimer, the same cycle based on structures after 200 ps of dynamics is shown in Figure 3(b). Again, the dimer in the membrane is the lowest energy state. Now that the various states have been allowed to relax, the observed energies of insertion and association are larger, and the energies of association differ only slightly from the effective interaction energies between the two helices (the reorganization energy is small). The magnitude of the interaction energies is exaggerated because of the use of energy-minimized structures. The average interaction energy from the dynamics of GpA in the membrane is -39 kcal/mol, compared to -51 using energy-minimized structures.

### Tyr and Trp at the Interface

In integral membrane protein structures, Trp and Tyr are very often observed near the hydrocarbon/headgroup interface.<sup>75,76</sup> The origin of this behavior is not entirely clear. A simple idea is that because Tyr and Trp, although predominantly hydrophobic, have polar groups that interact favorably with water, they are optimally located near the interface so that they can favorably solvate both their polar and nonpolar groups.<sup>77</sup> However, this view is in conflict with the observation that analogs of Trp that lack hydrogen-bonding capacity also prefer the interface and do not immerse more deeply in the membrane.<sup>78</sup>

The present model predicts the lowest energy position of Trp and Tyr side-chains to be at the interface (Table V) with the NH or OH group pointing toward water. In the model, this is a result of the amphipathicity mentioned above (i.e., a compromise between nonpolar solvation being optimal in the core and polar solvation being optimal in water). For Phe, the optimal position is in the hydrophobic core, consistent with observations that Phe behaves like an aliphatic residue.<sup>75</sup> The transfer free energies from water to the interface are -1.7, -1.8, and -1.7 kcal/mol for Trp, Tyr, and Phe, respectively. For comparison, the values extracted from experiments on the partitioning of

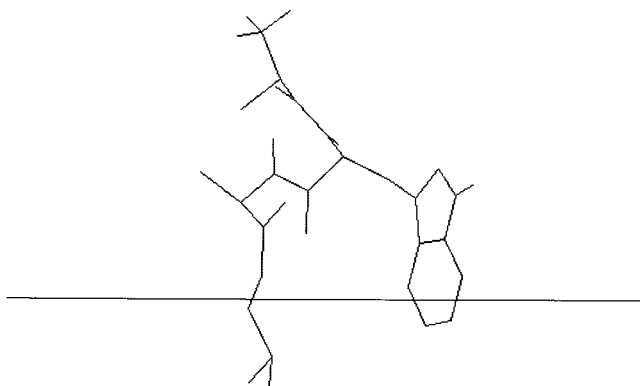


Fig. 4. Configuration of the Ala-Trp-Ala-O-tert-butyl peptide in the membrane.

small, unstructured peptides are  $-1.86$ ,  $-0.95$ , and  $-1.14$  kcal/mol, respectively.<sup>79</sup> These values are obtained by subtracting the contribution of Gly from the whole-residue transfer free energy.

To examine the preferred location of Trp in the context of a peptide, we simulated the tripeptide Ala-Trp-Ala-O-tert-butyl, whose binding thermodynamics and location in DOPC bilayers have been determined by Jacobs and White.<sup>80</sup> A 200-ps MD simulation of this peptide starting from an extended conformation produced a conformation with the tert-butyl group and the six-member Trp ring inserted into the membrane (Fig. 4). This conformation is about 3 kcal/mol lower than in water. This value is a bit low, considering that the experimental free energy of binding is  $-3$  kcal/mol (molar concentration scale) and includes an unfavorable translational/rotational entropy contribution. This position of the Trp side-chain is in agreement with the *minor* population seen by neutron diffraction<sup>80</sup> (a Gaussian centered at  $12.8$  Å; the center of mass of the Trp side-chain is  $14.5$  Å). The major (83%) population in the experiment, a broad Gaussian centered at the midplane between bilayers, is not seen in our model. This is possibly due to lack of explicit treatment of the headgroup region.

### C-Helix of Bacteriorhodopsin

The C-helix of bacteriorhodopsin is one of the few systems in which quantitative information on the thermodynamics of binding and insertion into membranes is available.<sup>81</sup> This helix is soluble in both aqueous solution and vesicles. In water it is unstructured, although the possibility of aggregation could not be excluded. At neutral pH, the peptide associates with membranes in a nonhelical, probably peripheral conformation. At pH 6.0, it undergoes a transition to a transbilayer helix, coupled with the protonation of one Asp residue (either Asp85 or Asp96). At pH 7, the free energy of binding at the peripheral location was measured to be  $-7.5$  kcal/mol and to the transbilayer location  $-6.1$  kcal/mol.<sup>81</sup>

This peptide was built as an ideal  $\alpha$ -helix and simulated in two locations: transbilayer and parallel to the surface

with the two Asp residues pointing toward water. A 50-ps simulation of the transbilayer location led to a configuration where Asp 96 was buried in the hydrocarbon core, Asp85 was at the hydrocarbon boundary, and Arg 81 was in the headgroup region [Fig. 5(a)]. Asp102 and Asp104 are at the other boundary. We can conclude that, as found by experiment, insertion is coupled to the protonation of only one Asp and can further propose that it is Asp96. A 400-ps simulation starting from the interfacial position led to a broken helix shown in Figure 5(b), with parts of a Leu, Pro, and Phe side-chains inserted.

The energies of these structures are shown in Table VI. To compare with the experimental free energy data, we need to account for the following three contributions. First, the loss of translational/rotational entropy of the peptide upon binding to the bilayer. A detailed analysis of the entropic terms is beyond the scope of this article. Previous work proposed values between  $3.7$  kcal/mol<sup>82</sup> and  $5$  kcal/mol<sup>13</sup> for the translational and orientational entropy. These authors also included a lipid perturbation free energy (about  $2$  kcal/mol), but one might argue that this is included in the solvation free energy. Second, the fact that the aqueous state of the peptide is not a helix. The free energy difference between coil and helix in solution for this peptide is not known. Assuming a value of  $2$  kcal/mol leads to 97% coil, a reasonable value. Third, a more accurate calculation of protonation/deprotonation energetics. The treatment of Asp96 as deprotonated in our model gives a desolvation energy cost of about  $14$  kcal/mol upon membrane insertion. The desolvation cost for a protonated Asp in our model is about  $6.5$  kcal/mol. Adding to that the free energy of protonation at neutral pH ( $4.3$  kcal/mol) gives about  $11$  kcal/mol. Therefore, our treatment of Asp96 as deprotonated overestimates the desolvation cost by about  $3$  kcal/mol. Given the above estimates, for rough agreement with experiment we should obtain a  $\Delta W$  between helix in water and TM helix of about  $-10$  kcal/mol. Instead, we obtain a  $\Delta W$  of  $+1$  kcal/mol. However, remembering that DMPC bilayers are a little thinner than other bilayers and using a value  $T = 23$  Å<sup>66</sup> instead of  $26$  Å, we obtain the second set of values that gives  $\Delta W = -7$  kcal/mol. This more favorable value is largely due to the better solvation of Asp 85 in the thinner bilayer. Although still smaller than the  $-10$  required, this value is satisfactorily close to experiment. More quantitative fine-tuning of the model will be performed in the future by considering a wider range of experimental data and using a more rigorous protocol in the calculations. On the basis of the above results, one might venture the prediction that the insertion free energy of BR-C would be less favorable in POPC bilayers.

The energy of the broken interfacial helix is more favorable than the TM configuration by  $-5$  kcal/mol ( $-2$  with the protonation correction). Although this value is close to the experimental free energy estimate, this is probably fortuitous. We cannot claim that the conformation shown in Figure 5(b) is realistic (actually, the experiment suggests an entirely nonhelical structure) and that entropic effects make no contributions. Nevertheless, the

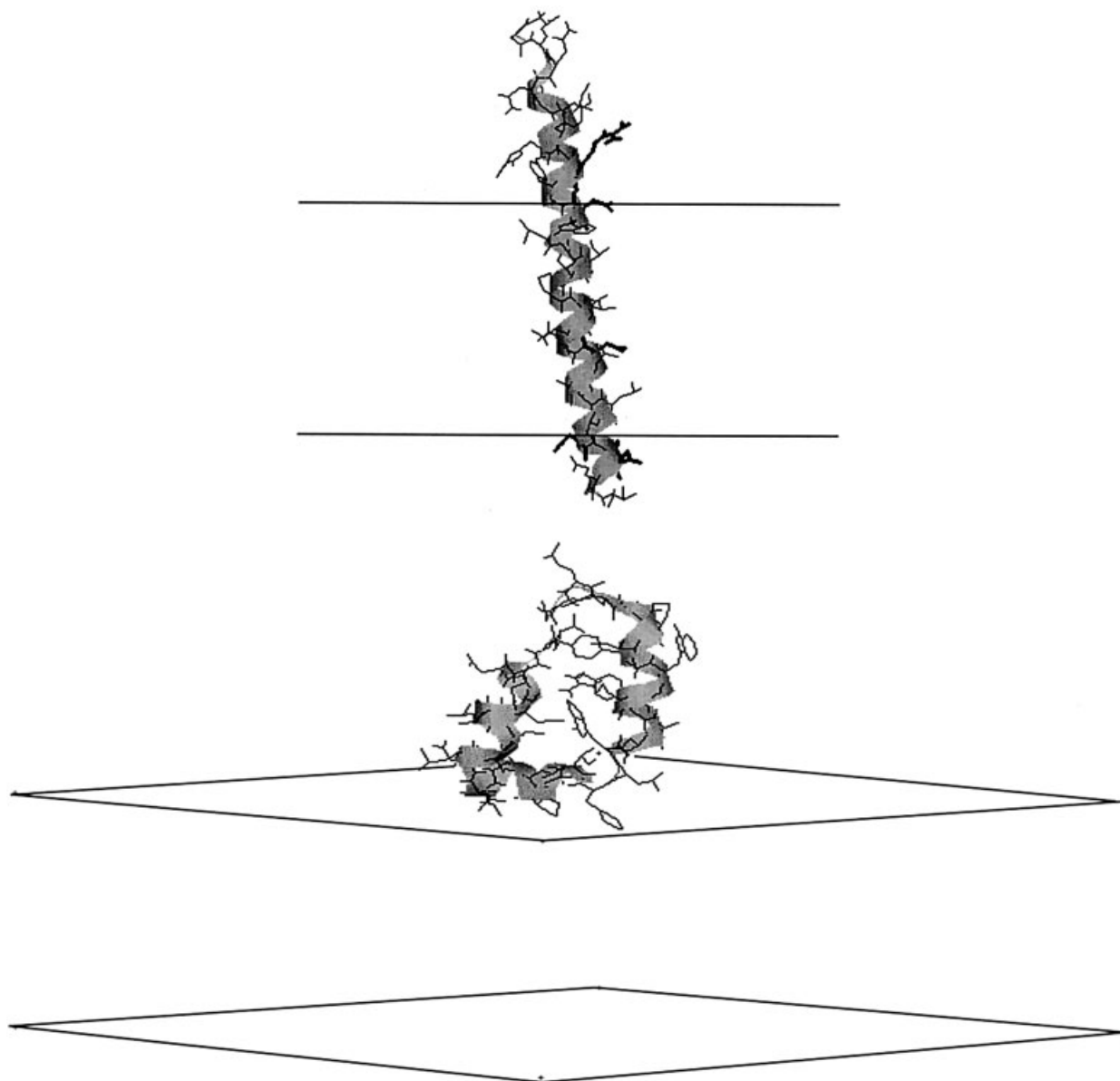


Fig. 5. The final position after MD of the C-helix of bacteriorhodopsin. **a:** TM position. Asp and Arg residues are shown in thick lines. **b:** Interfacial position.

simulation at the very least shows that a single helix is unstable, in contrast to the other amphipathic interfacial helices discussed below, and that the peptide interacts favorably with the membrane (it does not dissociate and has an energy lower than in water). Longer simulations could presumably lead to lower free energy states.

One final issue that needs to be considered when comparing with experimental data is temperature. The experiments on the C-helix were performed at 35°C, whereas the solvation parameters in our model correspond to 25°C. It is possible to use solvation enthalpy data to derive solvation parameters at other temperatures. This is accommodated for aqueous solvation in EEF1.<sup>51</sup> For solvation in cyclohexane, there are no solvation enthalpy data for amino acid

**TABLE VI. Effective Energies (kcal/mol) of Different Conformations of BR-C<sup>†</sup>**

	W (vdw, elec, solv)	$\Delta W$ from water
TM (T = 26Å)	-1011 (-208, -610, -282)	+1
Same conformation in water	-1012 (-208, -573, -320)	
TM (T = 23Å)	-1019 (-206, -607, -294)	-7
Interfacial	-1024 (-215, -572, -326)	-12

<sup>†</sup>Asp96 is treated as deprotonated. The values in parentheses are the van der Waals, electrostatic, and solvation free energy contributions.

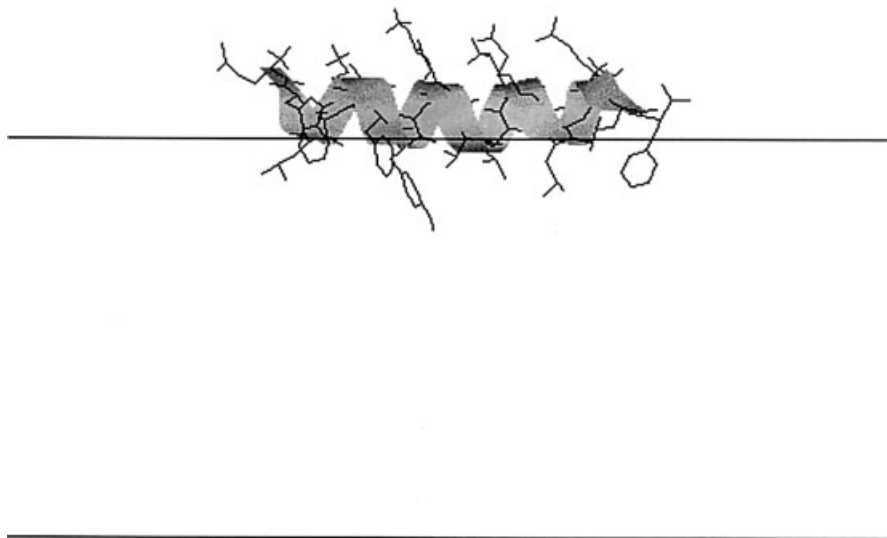


Fig. 6. The final conformation of 18A after MD simulation.

**TABLE VII. Energy of 18A in Different Configurations (kcal/mol)<sup>†</sup>**

	W (vdw, elec, solv)	$\Delta W$ from water
Interface	-575 (-119, -250, -240)	-7
Same conformation in water	-568 (-119, -244, -239)	
Transmembrane	-505 (-132, -290, -119)	+63

<sup>†</sup>The values in parentheses are the van der Waals, electrostatic, and solvation free energy contributions.

side-chains from gas to cyclohexane. We have used solvation enthalpies of hydrocarbons<sup>64</sup> to derive an enthalpy contribution of  $-1.16$  kcal/mol for a methylene group. Assuming then the same ratio of  $\Delta H^{\text{ref}}/\Delta G^{\text{ref}}$  for all atom types, we derived a tentative set of solvation enthalpy parameters for cyclohexane. Using these parameters, we calculated that at  $35^\circ\text{C}$  insertion will be favored by an extra kcal/mol, a rather small effect. One has to keep in mind, however, that solvation enthalpies for insertion into bilayers sometimes differ substantially from those for transfer from water to a bulk hydrocarbon.<sup>83</sup>

## 18A

18A is an amphipathic peptide that adsorbs on the bilayer surface.<sup>84,85</sup> The peptide was built as an ideal helix and placed parallel to the bilayer with the hydrophobic side inward. A 400-ps simulation resulted in a similar, surface adsorbed structure shown in Figure 6. A 400-ps simulation starting from a TM position was also performed. The peptide remained a TM helix. The energies of these structures are reported in Table VII. The surface-adsorbed structure has the lowest energy, lower by 7 kcal/mol than in water. The TM orientation has much higher energy due to the burial of several Lys and Glu side-chains on the polar face of the helix. The average  $z$

coordinate of all backbone carbonyl carbons is  $15.7 \text{ \AA}$ , compared to a position of the helix axis of  $17.1 \text{ \AA}$  found in a recent X-ray diffraction study<sup>85</sup> (the thickness of the DOPC bilayer used in this experiment is approximately equal to the  $26 \text{ \AA}$  used in the calculations).

## Melittin

Melittin is one of the most extensively studied membrane-binding peptides. It is the major component of bee venom that induces lysis of cell and model membranes. In aqueous solution at high ionic strength it forms tetramers,<sup>86</sup> whose structure has been determined.<sup>87</sup> In this structure, each peptide forms a bent amphipathic helix with the hydrophobic residues buried in the interior of the tetramer core. Its position and orientation in membranes seems to depend on experimental conditions. Although some studies found a transbilayer orientation,<sup>88-90</sup> other studies found a location at the interface with orientation parallel to the bilayer,<sup>91-93</sup> and other studies found both, depending on the conditions.<sup>94,95</sup> Recent all-explicit molecular dynamics simulations were based on different initial conformations, on the surface with inserted N-terminus,<sup>8</sup> transbilayer,<sup>9</sup> or a pore-forming tetramer.<sup>96</sup>

We first simulated this peptide as a transbilayer helix. One monomer from the crystal structure was placed in a TM orientation with its principal axis perpendicular to the bilayer plane. A 100-ps MD simulation led to the structure shown in Figure 7, which is very similar to the crystal structure (bRMSD  $1.6 \text{ \AA}$ , all atom RMSD  $2.9 \text{ \AA}$ ). Lys 7 “snorkels” to the same side as the N-terminus, whereas the remaining charged residues are on the other side. In the final structure, the kink angle between the two helical portions is  $131^\circ$  versus  $131$  and  $128^\circ$  in the two chains in the crystal (the original article reports an angle of about  $120^\circ$ .<sup>87</sup> The exact value depends on the way the calculation is performed). The tilt angle of the N-terminal helix is  $36^\circ$  and of the C-terminal helix  $15^\circ$ . A simulation with  $T = 23$

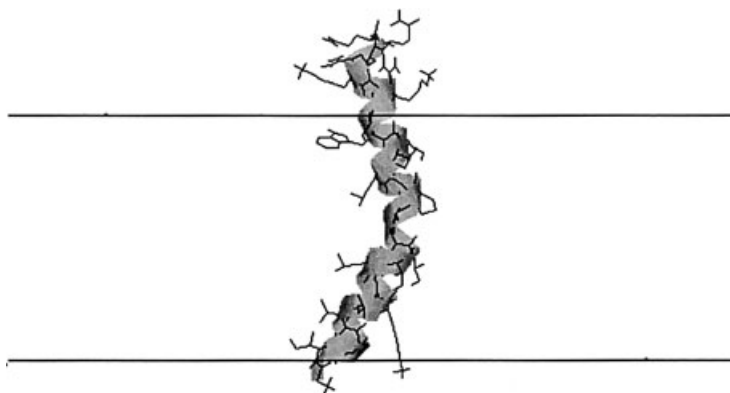


Fig. 7. Final transbilayer conformation of melittin.

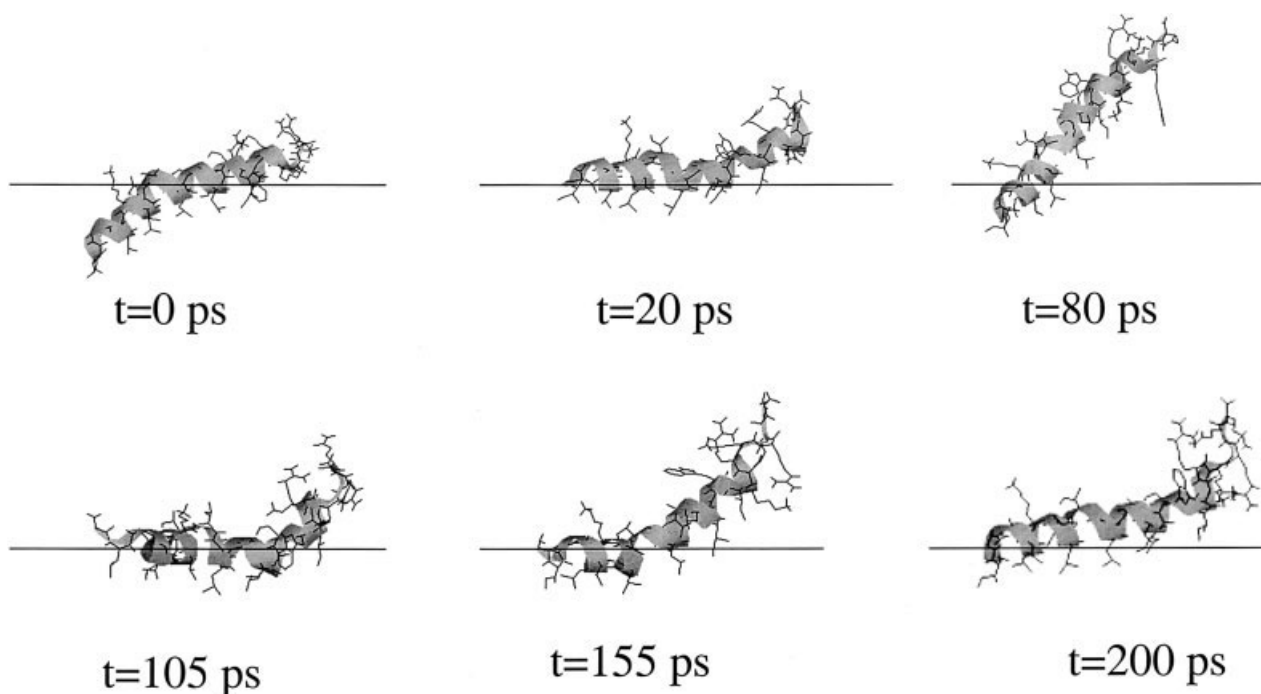


Fig. 8. Snapshots from the MD simulation of melittin at the interfacial position.

Å gave kink angle  $135^\circ$ , N-terminal tilt  $40^\circ$ , and C-terminal tilt  $10^\circ$ ). A solid-state NMR study of melittin in DMPC bilayers gave kink angle  $\sim 140$  or  $\sim 160^\circ$ , N-terminal tilt of  $30^\circ$ , and C-terminal tilt of  $10^\circ$ .<sup>88</sup>

Another simulation started from the “wedge” configuration proposed by Eisenberg and coworkers<sup>97</sup> and used as initial conformation by Bernéche et al.<sup>8</sup> This structure was first simulated for 30 ps with harmonic restraints on the backbone to allow the side-chains to relax. Subsequently, the restraints were released, and the simulation was continued for another 200 ps. Figure 8 shows characteristic snapshots from this simulation. The N-terminus rapidly moves out of the hydrocarbon core. Large fluctuations in the position and the orientation of the helix are observed during the simulation. In the final structure, the entire peptide remains helical except for the C-terminal turn,

where the  $\alpha$ -helical hydrogen bonds are replaced by side-chain-backbone hydrogen bonds. This is consistent with experiments that showed that the five C-terminal residues are not helical.<sup>93,98</sup> The kink angle as a function of time is shown in Figure 9. The average kink angle is calculated to be  $145^\circ$ , larger than in the crystal or the TM orientation. This tends to agree with the X-ray diffraction data<sup>92</sup> but not the NOE analysis.<sup>98</sup> Because a straight helix has been proposed as the best fit to the diffraction data, a third simulation started from a straight, ideal  $\alpha$ -helix at the interface with the hydrophobic side inward. This simulation gave an average kink angle within statistical uncertainty from that of the previous simulation (the kink developed within 10 ps). Thus, the simulations support a less kinked conformation at the interface, but not an entirely straight helix. A more thorough comparison of the

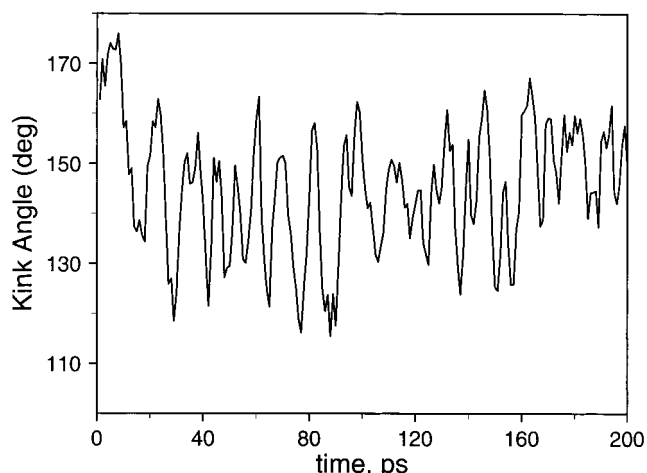


Fig. 9. The kink angle as a function of time from the MD simulation of melittin at the interfacial position.

conformational ensemble observed here and the scattering densities from X-ray diffraction is needed to resolve this discrepancy. The larger kink angle may be caused by the tendency of the termini to move into water and the tendency of the hydrophobic side-chains in the middle of the helix to move deeper into the membrane.

A spin labeling study<sup>91</sup> reported that the order of solvent accessibility of the Lysines and N-terminus is  $\text{Lys23} < \text{N-term} < \text{Lys21} < \text{Lys7}$ . In our final structure, Lys 7 is clearly the most accessible, followed by the N-terminus. Lys 21 and 23 seem equally accessible. As mentioned above, ideally one should examine a large ensemble of conformations, instead of just one. Again, these more thorough comparisons are left for future publications.

The energies of the various conformations of melittin (with protonated N-terminus) are shown in Table VIII. Here average energies from the last 5 ps of the simulation are also reported in parentheses and show the variations in calculated energy differences with protocol. Lowest in energy is the TM position for a bilayer of  $T = 23 \text{ \AA}$ , about 11 kcal/mol lower than a helix in water, based on average energies. Second in energy is the interfacial position, and next the TM position in the  $T = 26 \text{ \AA}$  bilayer, which is slightly favored over a helix in water. The lower energy in the  $T = 23 \text{ \AA}$  bilayer is due to smaller desolvation cost of the polar and charged residues near the C-terminus. These results suggest that some of the experimental discrepancies regarding melittin's orientation may be due to differences in bilayer thickness. Indeed, some experiments that find melittin at the interface seem to use longer lipids,<sup>91,92</sup> and some experiments that find TM orientations use shorter lipids.<sup>88-90</sup> Lower levels of bilayer hydration<sup>94</sup> may also affect the optimal orientation by reducing the desolvation cost for the polar and charged residues at the C-terminus. Another factor that should be kept in mind is that some experiments use high enough concentrations of melittin that interactions between monomers in the membrane could be present, affecting the preferred orientation.

Such interactions have been neglected in the above calculations.

Experiments give an estimate of  $-7$  to  $-8$  kcal/mol for partitioning of melittin to the membrane interface ( $-5$  to  $-6$  at 1 M standard state).<sup>99</sup> Our average energies give  $-5$  kcal/mol, which seems a bit low given that we do not include the entropy of adsorption and the difference in free energy between helix and coil in water. We could note at this point that the affinity of melittin for anionic membranes is two orders of magnitude larger than for zwitterionic membranes. The current model neglects any electrostatic effects with the headgroups; the above results pertain to zwitterionic membranes.

### Bacteriorhodopsin

Bacteriorhodopsin was simulated without the retinal. The residues Asp96 and Asp212 were treated as protonated.<sup>101</sup> A 200-ps MD simulation gave a bRMSD of  $2.96 \text{ \AA}$  for all residues and  $2.06 \text{ \AA}$  for the TM portion. Most of the movement occurred in the loops on both sides of the membrane (Fig. 10). For comparison, a simulation in vacuum of the same duration gave bRMSD of  $3.7 \text{ \AA}$  ( $2.5 \text{ \AA}$  for the TM portion) and a simulation in implicit water gave  $3.1 \text{ \AA}$  ( $2.6 \text{ \AA}$  for the TM portion). A simulation with  $T = 30 \text{ \AA}$  gave  $3.1 \text{ \AA}$  bRMSD ( $2.24 \text{ \AA}$  for the TM portion). Table IX shows the tilt angles of the seven helices before and after the simulations.

Table 10 shows the effective energies of BR in the membrane and in water. For the crystal structure, the energy of insertion is just  $-11$  kcal/mol. Energy minimization and dynamics optimize the conformation for the model membrane and enhance this difference. The difference in average energy between a simulation in membrane and a simulation in water is  $-88$  kcal/mol.

### DISCUSSION

The tests reported above show that a useful model for peptides and proteins in membranes has been obtained with bulk solvation free energy data and a simple adjustment of the electrostatic interactions in the membrane. The main difference of the present function from previous efforts is that it is coupled to an effective energy function in water, rather than a vacuum force field, and that it is capable of providing the difference in energy between different conformations, as well as between different positions. That is, it can provide information not only on the vertical steps of the thermodynamic cycle of Figure 3 but also on the horizontal steps. The function that is closest in spirit to IMM1 is the recent extension of the Generalized Born model to membranes.<sup>102</sup> Far from the membrane, this model reduces to the standard Generalized Born model for aqueous proteins. The published results are not sufficient to assess the quantitative performance of this model. IMM1 is also similar to the model of Efremov and coworkers based on atomic solvation parameters.<sup>27,32,33</sup> The main differences are the use of solvent-accessible surface areas by that model, rather than pairwise contacts, and the lack of adjustment of the electrostatic interactions in the membrane. Again, not enough thermo-

**TABLE VIII. Energy of Melittin in Different Configurations (Protonated N-Terminus)**

	$W_{\min}$ (vdw, elec, solv)	$\langle W \rangle$ (vdw, elec, solv)	$\Delta\langle W \rangle$ from water
Water	-711 (-143, -384, -243)	-498 (-132, -357, -249)	
Interface	-723 (-135, -396, -255)	-503 (-120, -372, -259)	-5
TM T = 26 Å	-715 (-128, -440, -208)	-500 (-115, -406, -216)	-2
TM T = 23 Å	-735 (-129, -447, -221)	-509 (-115, -414, -226)	-11

$\langle W \rangle$  is the average effective energy over the last 5 ps of dynamics. All values are in kcal/mol.

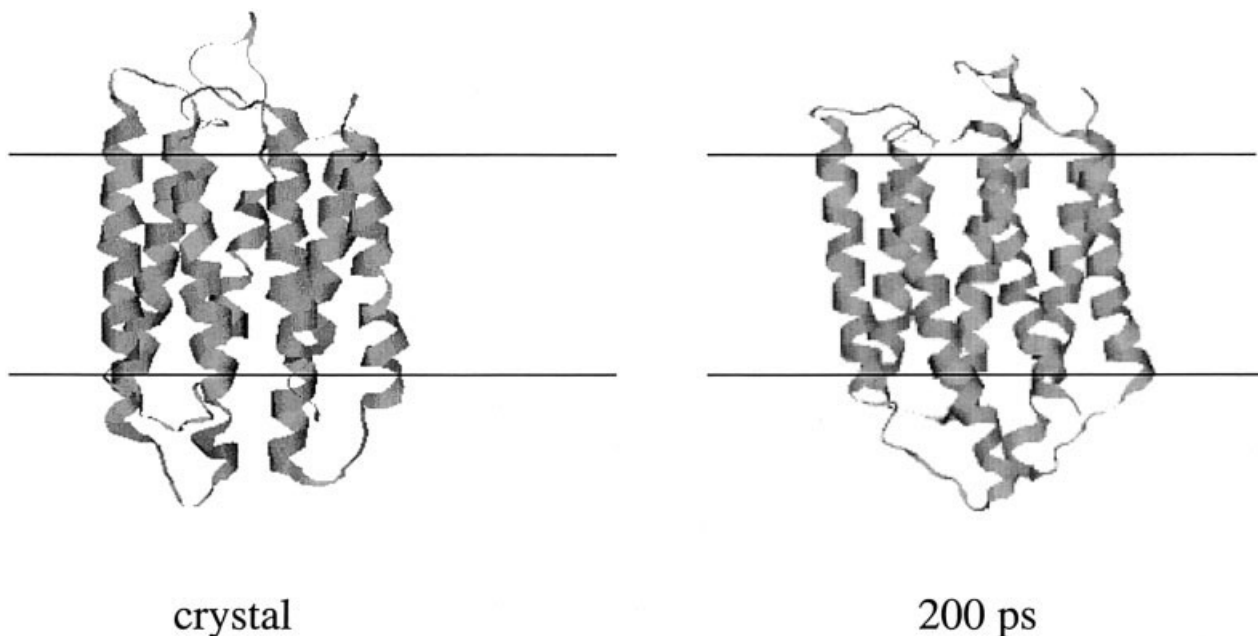


Fig. 10. Initial and final (after MD simulation) conformation of bacteriorhodopsin.

**TABLE IX. Tilt Angles of the Bacteriorhodopsin Helices Before and After Simulations**

Helix	Crystal <sup>a</sup>	T = 26 Å simulation	T = 30 Å simulation
A	24	17	20
B	14	17	15
C	13	15	10
D	13	19	12
E	7	9	9
F	3	16	21
G	6	18	13

<sup>a</sup>The tilt is not known from the experiment. This value results from placing the protein with its principal axis along the bilayer normal.

dynamic data have been reported to make a more detailed comparison of performance.

The most empirical aspect of the energy function is the model adopted for the change in dielectric constant in the membrane. Physically, the strengthening of electrostatic interactions in a nonpolar environment is undoubtedly correct, but the form adopted is not theoretically justified. Here we tried to make a model that is compatible with the linear distance-dependent dielectric in water. Efforts for a better dielectric screening function should be coordinated with implementation of a more realistic screening function

in aqueous proteins. One approach toward that end is to generate a large amount of effective dielectric constant data in the membrane by using continuum electrostatics and fit the data to an approximate analytical function, as was done for globular proteins.<sup>103</sup>

Another questionable aspect is the treatment of the headgroup area (the interface) as having the same properties as water. It would be a simple extension to treat the interface as a separate “phase.” The true difficulty is the lack of data on the solvent properties of the interface. Although experimental data for the binding of peptides exist,<sup>79,104</sup> their use for our purposes is hampered by the lack of knowledge as to the exact location of their side-chains. Nevertheless, they could be used to create a tentative model for the interface. An alternative, theoretical approach to obtaining such data is through free energy simulations. Some studies of that nature have already been reported,<sup>105,106</sup> but many more studies are needed. These data can be incorporated in the model in a straightforward way. For example, the  $f(z)$  profile does not have to be the same for all groups and does not have to be monotonic. One advantage of the present approach over Poisson–Boltzmann (other than computational speed) is the decoupling of the calculation of self-energies from the calculation of interaction energies, which provides more

**TABLE X. Energy of BR Conformations (kcal/mol)**

	Total (vdw, elec, solv)	Same conformation in water
Crystal	-3935 (-753, -2869, -1068)	-3924 (-753, -2621, -1304)
Minimized crystal	-5447 (-1556, -3352, -1101)	-5416 (-1556, -3095, -1328)
Minimized dynamics	-5808 (-1631, -3603, -1069)	-5416 (-1631, -3334, -1276)
Average dynamics	-3882 (-1447, -3373, -1131)	
Water minimized	-5746 (-1640, -3265, -1327)	
Water average	-3794 (-1451, -3051, -1398)	

flexibility in the direct incorporation of experimental data. Moreover, the optimal values of  $\epsilon$  for self-energies and for interaction energies may not be the same.<sup>107</sup>

The quantitative performance of this initial parameterization of IMM1 is quite good, although in a few cases we obtained insertion energies that are a bit too low. The model will be further calibrated against available thermodynamic data. For quantitative comparison with experimental free energies of membrane binding, we need good estimates of the translational/rotational/conformational entropy of binding, which are not included in  $\Delta W$ . Such estimates have been made for TM helices,<sup>13,82</sup> and these can be extended to interfacial binding. The model parameters that can be easily adjusted to improve quantitative performance are mainly  $a$  in Eq. 10 and  $n$  in Eq. 7.

The present function cannot be yet applied to proteins containing aqueous channels, such as ion channels, because any empty space within the slab is supposed to be occupied by lipid and the insertion of such a protein into the membrane would be unfavorable because of the desolvation of the polar and charged residues lining the pore. A straightforward extension of the model would be to embed an implicit aqueous cylinder into the membrane, as was done for Poisson–Boltzmann calculations.<sup>19</sup> The model, in its present form, also does not apply to lipids that carry a net charge but can easily be extended to incorporate the electrostatic effects of such headgroups. For zwitterionic lipids, the “dipole potential” was calculated by La Rocca et al.<sup>37</sup> A similar calculation using continuum electrostatics could be performed for anionic lipids, or one could use the Gouy–Chapman theory.<sup>108</sup> One of the limitations of all hydrophobic slab models is that they do not allow for deformation of the membrane by the proteins. Membrane deformation occurs when it lowers the free energy of the system. Therefore, its neglect will underestimate the tendency of peptides to partition into the membrane.

This energy function could find use in structure prediction efforts for membrane proteins, especially in simple cases such as the structure of associated TM helices. So far, most efforts in this area have relied on a vacuum force field. In their simulated annealing studies, Brunger and coworkers identified several low-energy configurations and selected among them based on experimental data.<sup>43,44,109</sup> An energy function that takes into account solvation by lipids and the heterogeneity of the membrane environment should in principle perform better and could perhaps be able to distinguish among those low-energy configurations. For that purpose, we would need to establish that the experimental structure of such helix dimers

corresponds to the global minimum of our energy function. Stable MD simulations only show that it is a local minimum.

A second important application could be the exploration of possible positions, orientations, and conformations of membrane active peptides, such as antimicrobial peptides, Alzheimer’s disease-related peptides, or viral fusion peptides. As shown by the BR-C and melittin test cases, this type of modeling can be useful in interpreting experimental data. The optimal arrangements found by this function could be used as initial configurations for all-atom simulations.

## ACKNOWLEDGMENT

We thank Dr. S.O. Smith for providing the coordinates of GpA before deposition to the PDB.

## REFERENCES

- Egberts E, Berendsen HJC. MD simulation of a smectic liquid crystal with atomic detail. *J Chem Phys* 1988;89:3718–3732.
- Heller H, Schaefer M, Schulten K. MD simulation of a bilayer of 200 lipids in the gel and in the liquid-crystal phases. *J Phys Chem* 1993;97:8343–8360.
- Venable RM, Zhang Y, Hardy BJ, Pastor RW. MD simulations of a lipid bilayer and of hexadecane: an investigation of membrane fluidity. *Science* 1993;262:223–226.
- Tu K, Klein ML, Tobias DJ. Constant-pressure and temperature MD simulation of a fully hydrated liquid crystal phase DPPC bilayer. *Biophys J* 1995;69:2558–2562.
- Biggin PC, Sansom MSP. Interactions of  $\alpha$ -helices with lipid bilayers: a review of simulation studies. *Biophys Chem* 1999;76: 161.
- Woolf TB, Roux B. MD simulation of the gramicidin channel in a phospholipid bilayer. *Proc Natl Acad Sci USA* 1994;91:11631–11635.
- Edholm O, Berger O, Jähnig F. Structure and fluctuations of bacteriorhodopsin in the purple membrane: a MD study. *J Mol Biol* 1995;250:94–111.
- Bernéche S, Nina M, Roux B. MD simulation of melittin in a DMPC bilayer membrane. *Biophys J* 1998;75:1603–1618.
- Bachar M, Becker OM. Protein-induced membrane disorder: a MD study of melittin in a DPPC bilayer. *Biophys J* 2000;78:1359–1375.
- Tieleman DP, Berendsen HJC. A MD study of the pores formed by E. Coli OmpF porin in a fully hydrated POPC bilayer. *Biophys J* 1998;74:2786–2801.
- Tu K, Klein ML, Tobias DJ. Constant-pressure MD investigation of cholesterol effects in a DPPC bilayer. *Biophys J* 1998;75:2147–2156.
- Petrache HI, Grossfield A, MacKenzie KR, Engelman DM, Woolf TB. Modulation of glycophorin A transmembrane helix interactions by lipid bilayers: molecular dynamics simulations. *J Mol Biol* 2000;302:727–746.
- Ben-Tal N, Ben-Shaul A, Nicholls A, Honig B. Free energy determinants of  $\alpha$ -helix insertion into lipid bilayers. *Biophys J* 1996;70:1803–1812.
- Kessel A, Cafiso DS, Ben-Tal N. Continuum solvent model

- calculations of alamethicin-membrane interactions: thermodynamic aspects. *Biophys J* 2000;78:571–583.
15. Bechor D, Ben-Tal N. Implicit solvent model studies of the interactions of the influenza hemagglutinin fusion peptide with lipid bilayers. *Biophys J* 2001;80:643–655.
  16. Kessel A, Musafia B, Ben-Tal N. Continuum solvent model studies of the interactions of an anticonvulsant drug with a lipid bilayer. *Biophys J* 2001;80:2536–2545.
  17. Murray D, Ben-Tal N, Honig B, McLaughlin S. Electrostatic interaction of myristoylated proteins with membranes: simple physics, complicated biology. *Structure* 1997;5:985–989.
  18. Murray D, McLaughlin S, Honig B. The role of electrostatic interactions in the membrane association of G protein by heterodimers. *J Biol Chem* 2001;276:45153–45159.
  19. Roux B, MacKinnon R. The cavity and pore helices of the KcsA K<sup>+</sup> channel: electrostatic stabilization of monovalent cations. *Science* 1999;285:100–102.
  20. Ducarme P, Rahman M, Brasseur R. IMPALA: a simple restraint field to simulate the biological membrane in molecular structure studies. *Proteins* 1998;30:357–371.
  21. Brasseur R, Deleers M, Malaisse WJ, Ruysschaert J-M. Conformational analysis of the Ca-A23187 complex at a lipid-water interface. *Proc Natl Acad Sci USA* 1982;79:2895–2897.
  22. Brasseur R, Pillot T, Lins L, Vandekerckhove J, Rosseneu M. Peptides in membranes: tipping the balance of membrane stability. *Trends Biochem Sci* 1997;22:167–171.
  23. Jahnig F, Edholm O. Modeling of the structure of bacteriorhodopsin. *J Mol Biol* 1992;226:837–850.
  24. Ram P, Kim E, Thomson DS, Howard KP, Prestegard JH. Computer modeling of glycolipids at membrane surfaces. *Biophys J* 1992;63:1530–1535.
  25. Sanders CR, Schwonek JP. An approximate model and empirical energy function for solute interactions with a water-phosphatidylcholine interface. *Biophys J* 1993;65:1207–1218.
  26. Milik M, Skolnick J. Spontaneous insertion of peptide chains into lipid membranes: an off-lattice Monte Carlo dynamics model. *Proteins* 1993;15:10–25.
  27. Efremov RG, Nolde DE, Vergoten G, Arseniev AS. A solvent model for simulations of peptides in bilayers. I. Membrane-promoting  $\alpha$ -helix formation. *Biophys J* 1999;76:2448–2459.
  28. Milik M, Skolnick J. Spontaneous insertion of polypeptide chains into membranes: a Monte Carlo model. *Proc Natl Acad Sci USA* 1992;89:9391–9395.
  29. Baumgartner A. Insertion and hairpin formation of membrane proteins: a Monte Carlo study. *Biophys J* 1996;71:1248–1255.
  30. Maddox MW, Longo ML. A Monte Carlo study of peptide insertion into lipid bilayers: equilibrium conformations and insertion mechanisms. *Biophys J* 2002;82:244–263.
  31. Orlandini E, Seno F, Banavar JR, Laio A, Maritan A. Deciphering the folding kinetics of transmembrane helical proteins. *Proc Natl Acad Sci USA* 2000;97:14229–14234.
  32. Nolde DE, Arseniev AS, Vergoten G, Efremov RG. Atomic solvation parameters for protein in a membrane environment. *J Biomol Struct Dyn* 1997;15:1–18.
  33. Efremov RG, Nolde DE, Vergoten G, Arseniev AS. A solvent model for simulations of peptides in bilayers. II. Membrane-spanning  $\alpha$ -helices. *Biophys J* 1999;76:2460–2471.
  34. Volynsky PE, Nolde DE, Arseniev AS, Efremov RG. Monte Carlo simulation of peptides in membrane using heterogeneous implicit solvation model. *Internet J Chem* 1999;2:4.
  35. Efremov RG, Nolde DE, Volynsky PE, Chernyavsky AA, Dubovskii PV, Arseniev AS. Factors important for fusogenic activity of peptides: molecular modeling study of analogs of fusion peptide of influenza virus hemagglutinin. *FEBS Lett* 1999;462:205–210.
  36. Efremov RG, Volynsky PE, Nolde DE, Dubovskii PV, Arseniev AS. Interactions of cardiotoxins with membranes: a molecular modeling study. *Biophys J* 2002;83:144–153.
  37. La Rocca P, Sansom MSP. Peptide-bilayer interactions: simulations of dermaseptin B, an antimicrobial peptide. *Biophys Chem* 1999;76:145–159.
  38. Grossfield A, Sachs J, Woolf TB. Dipole lattice membrane model for protein calculations. *Proteins* 2000;41:211–223.
  39. Luo X, Zhang D, Weinstein H. Ligand-induced domain motion in the activation mechanism of a G-protein-coupled receptor. *Protein Eng* 1994;7:1441–1448.
  40. Strahs D, Weinstein H. Comparative modeling and molecular dynamics studies of the  $\delta$ ,  $\kappa$ , and  $\mu$  opioid receptors. *Protein Eng* 1997;10:1019–1038.
  41. Tuffery P, Etchebest C, Popot J-L, Lavery R. Prediction of the positioning of the seven transmembrane  $\alpha$ -helices of bacteriorhodopsin. *J Mol Biol* 1994;236:1105–1122.
  42. Pappu RV, Marshall GR, Ponder JW. A potential smoothing algorithm accurately predicts transmembrane helix packing. *Nat Struct Biol* 1999;6:50–55.
  43. Treutlein HR, Lemmon MA, Engelman DM, Brunger AT. The glycoporphin A transmembrane domain dimer: sequence-specific propensity for a right-handed supercoil of helices. *Biochemistry* 1992;31:12726–12733.
  44. Adams PD, Engelman DM, Brunger AT. Improved prediction for the structure of the dimeric transmembrane domain of glycoporphin A obtained through global searching. *Proteins* 1996;26:257–261.
  45. MacKenzie KR, Prestegard JH, Engelman DM. A transmembrane helix dimer: structure and implications. *Science* 1997;276:131–133.
  46. Sajot N, Genest M. Dimer interface of transmembrane domains for neu/erbB-2 receptor dimerization and transforming activation: a model revealed by MD simulations. *J Biomol Struct Dyn* 2001;19:15–31.
  47. Herzyk P, Hubbard RE. Combined biophysical and biochemical information confirms arrangement of transmembrane helices visible from the three-dimensional map of frog rhodopsin. *J Mol Biol* 1998;281:741–754.
  48. Filizola M, Carteni-Farina M, Perez JJ. Modeling the 3D structure of rhodopsin using a de novo approach to build G-protein-coupled receptors. *J Phys Chem B* 1999;103:2520–2527.
  49. Palczewski K, Kumasaka T, Hori T, Behnke CA, Motosima H, Fox BA, Le Trong I, Teller DC, Okada T, Stenkamp RE, Yamamoto M, Miyano M. Crystal structure of rhodopsin: a G protein-coupled receptor. *Science* 2000;289:739–745.
  50. Lazaridis T, Karplus M. “New view” of protein folding reconciled with the old through multiple unfolding simulations. *Science* 1997;278:1928–1931.
  51. Lazaridis T, Karplus M. Effective energy function for proteins in solution. *Proteins* 1999;35:133–152.
  52. Neria E, Fischer S, Karplus M. Simulation of activation free energies in molecular systems. *J Chem Phys* 1996;105:1902–1921.
  53. Lazaridis T, Karplus M. Discrimination of the native from misfolded protein models with an energy function including implicit solvation. *J Mol Biol* 1999;288:477–487.
  54. Dinner AR, Lazaridis T, Karplus M. Understanding  $\beta$ -hairpin folding. *Proc Natl Acad Sci USA* 1999;96:9068–9073.
  55. Paci E, Smith LJ, Dobson CM, Karplus M. Exploration of partially unfolded states of human  $\alpha$ -lactalbumin by MD simulations. *J Mol Biol* 2001;306:329–347.
  56. Inuzuka Y, Lazaridis T. On the unfolding of  $\alpha$ -lytic protease and the role of the pro region. *Proteins* 2000;41:21–32.
  57. Paci E, Karplus M. Unfolding proteins by external forces and temperature: the importance of topology and energetics. *Proc Natl Acad Sci USA* 2000;97:6521–6526.
  58. Paci E, Karplus M. Forced unfolding of fibronectin type 3 modules: an analysis by biased MD simulations. *J Mol Biol* 1999;288:441–449.
  59. Kumar S, Sham YY, Tsai C-J, Nussinov R. Protein folding and function: the N-terminal fragment in adenylate kinase. *Biophys J* 2001;80:2439–2454.
  60. Levy Y, Jortner J, Becker OM. Solvent effects on the energy landscape and folding kinetics of polyalanine. *Proc Natl Acad Sci USA* 2001;98:2188–2193.
  61. Masunov A, Lazaridis T. Potentials of mean force between ionizable amino acid sidechains in aqueous solution. *J Am Chem Soc* 2003;125:1722–1730.
  62. Fauchère J-L, Pliska V. Hydrophobic parameters of amino-acid side-chains from the partitioning of N-acetyl-amino-acid amides. *Eur J Med Chem-Chim Ther* 1983;18:369–375.
  63. Radzicka A, Wolfenden R. Comparing the polarities of the amino acids: side-chain distribution coefficients between the vapor phase, cyclohexane, 1-octanol, and neutral aqueous solution. *Biochemistry* 1988;27:1664–1670.
  64. Ben-Naim A, Marcus Y. Solvation thermodynamics of nonionic solutes. *J Chem Phys* 1984;81:2016–2027.
  65. Press WH, Flannery BP, Teukolsky SA, Vetterling WT. Numerical

- cal recipes, Fortran version. Cambridge: Cambridge University Press; 1989.
66. Rand RP, Parsegian VA. Hydration forces between phospholipid bilayers. *BBA* 1989;988:351–376.
  67. Wiener MC, White SH. Structure of a fluid dioleoylphosphatidylcholine bilayer determined by joint refinement of x-ray and neutron diffraction data. II. Distribution and packing of terminal methyl groups. *Biophys J* 1992;61:428–433.
  68. Bechinger B. Membrane insertion and orientation of polyalanine peptides: a <sup>15</sup>N solid-state NMR investigation. *Biophys J* 2001;81:2251–2256.
  69. Moll TS, Thompson TE. Semisynthetic proteins: model systems for the study of the insertion of hydrophobic peptides into preformed lipid bilayers. *Biochemistry* 1994;33:15469–15482.
  70. Chung LA, Thompson TE. Design of membrane-inserting peptides: spectroscopic characterization with and without lipid bilayers. *Biochemistry* 1996;35:11343–11354.
  71. Lewis RNAH, Zhang Y-P, Hodges RS, Subczynski WK, Kusumi A, Flach CR, Mendelsohn R, McElhaney RN. A polyalanine-based peptide cannot form a stable transmembrane  $\alpha$ -helix in fully hydrated phospholipid bilayers. *Biochemistry* 2001;40:12103–12111.
  72. Gurezka R, Laage R, Brosig B, Langosch D. A heptad motif of leucine residues found in membrane proteins can drive self-assembly of artificial transmembrane segments. *J Biol Chem* 1999;274:9265–9270.
  73. Smith SO, Eilers M, Song D, Crocker E, Ying W, Groesbeek M, Metz G, Ziliox M, Aimoto S. Implications of threonine hydrogen bonding in the glycoporphin A transmembrane helix dimer. *Biophys J* 2002;82:2476–2486.
  74. Smith SO, Song D, Shekar S, Groesbeek M, Ziliox M, Aimoto S. Structure of the transmembrane dimer interface of Glycophorin A in membrane bilayers. *Biochemistry* 2001;40:6553–6558.
  75. von Heijne G. Recent advances in the understanding of membrane protein assembly and structure. *Q Rev Biophys* 1999;32:285–307.
  76. White SH, Wimley WC. Membrane protein folding and stability: physical principles. *Annu Rev Biophys Biomol Struct* 1999;28:319–365.
  77. Schiffer M, Chang CH, Stevens FJ. The functions of Trp residues in membrane proteins. *Protein Eng* 1992;5:213–214.
  78. Yau W-M, Wimley WC, Gawrisch K, White SH. The preference of tryptophan for membrane interfaces. *Biochemistry* 1998;7:14713–14718.
  79. Wimley WC, White SH. Experimentally determined hydrophobicity scale for proteins at membrane interfaces. *Nat Struct Biol* 1996;3:842–848.
  80. Jacobs RE, White SH. The nature of the hydrophobic binding of small peptides at the bilayer interface: implications for the insertion of transbilayer helices. *Biochemistry* 1989;28:3421–3437.
  81. Hunt JF, Rath P, Rothschild KJ, Engelman DM. Spontaneous, pH-dependent membrane insertion of a transbilayer  $\alpha$ -helix. *Biochemistry* 1997;36:15177–15192.
  82. Ben-Shaul A, Ben-Tal N, Honig B. Statistical thermodynamic analysis of peptide and protein insertion into lipid membranes. *Biophys J* 1996;71:130–137.
  83. Wimley WC, White SH. Membrane partitioning: distinguishing bilayer effects from the hydrophobic effect. *Biochemistry* 1993;32:6307–6312.
  84. Lund-Katz S, Anantharamaiah GM, Venkatachalapathi YV, Segrest JP, Phillips MC. NMR investigation of the interactions with phospholipid of an amphipathic  $\alpha$ -helix-forming peptide of the apolipoprotein class. *J Biol Chem* 1990;265:12217–12223.
  85. Hristova K, Wimley WC, Mishra VK, Anantharamaiah GM, Segrest JP, White WH. An amphipathic  $\alpha$ -helix at a membrane interface: a structural study using a novel X-ray diffraction method. *J Mol Biol* 1999;290:99–117.
  86. Wilcox W, Eisenberg D. Thermodynamics of melittin tetramerization determined by circular dichroism and implications for protein folding. *Protein Sci* 1992;1:641–653.
  87. Terwilliger TC, Eisenberg D. The structure of melittin. II. Interpretation of the structure. *J Biol Chem* 1982;257:6016–6022.
  88. Naito A, Nagao T, Norisada K, Mizuno T, Tuzi S, Saito H. Conformation and dynamics of melittin bound to magnetically oriented lipid bilayers by solid state NMR. *Biophys J* 2000;78:2405–417.
  89. Smith R, Separovic F, Milne TJ, Whittaker A, Bennett FM, Cornell BA, Makriyannis A. Structure and orientation of the pore-forming peptide melittin in lipid bilayers. *J Mol Biol* 1994;241:456–466.
  90. Weaver AJ, Kemple MD, Brauner JW, Mendelsohn R, Prendergast FG. Fluorescence, CD, ATR FTIR, and <sup>13</sup>C NMR characterization of the structure and dynamics of synthetic melittin and melittin analogues in lipid environments. *Biochemistry* 1992;31:1301–1313.
  91. Altenbach C, Froncisz W, Hyde JS, Hubbell WL. Conformation of spin-labeled melittin at membrane surfaces investigated by EPR. *Biophys J* 1989;56:1183–1191.
  92. Hristova K, Dempsey CE, White WH. Structure, location, and lipid perturbations of melittin at the membrane interface. *Biophys J* 2001;80:801–811.
  93. Dempsey CE, Butler GS. Helical structure and orientation of melittin in dispersed phospholipid membranes from amide exchange analysis in situ. *Biochemistry* 1992;31:11973–11977.
  94. Frey S, Tamm LK. Orientation of melittin in phospholipid bilayers: a polarized ATR study. *Biophys J* 1991;60:922–930.
  95. Bradshaw JP, Dempsey CE, Watts A. A combined x-ray and neutron diffraction study of selectively deuterated melittin in phospholipid bilayers: effect of pH. *Mol Membr Biol* 1994;11:79–86.
  96. Lin J-H, Baumgaertner A. Stability of a melittin pore in a lipid bilayer: a MD study. *Biophys J* 2000;78:1714–1724.
  97. Terwilliger TC, Weissman L, Eisenberg D. The structure of melittin in the form I crystals and its implication for melittin's lytic and surface activities. *Biophys J* 1982;37:353–361.
  98. Okada A, Wakamatsu K, Miyazawa T, Higashijima T. Vesicle-bound conformation of melittin: TRNOE analysis in the presence of perdeuterated PC vesicles. *Biochemistry* 1994;33:9438–9446.
  99. Ladokhin AS, White SH. Folding of amphipathic  $\alpha$ -helices on membranes: energetics of helix formation by melittin. *J Mol Biol* 1999;285:1363–1369.
  100. Batenburg AM, van Esch JH, de Kruijff B. Melittin-induced changes of the macroscopic structure of PE. *Biochemistry* 1988;27:2324–2331.
  101. Gerwert K, Hess B, Soppa J, Oesterhelt D. Role of Asp-96 in proton translocation by bacteriorhodopsin. *Proc Natl Acad Sci USA* 1989;86:4943–4947.
  102. Spassov VZ, Yan L, Szalma S. Introducing an implicit membrane in Generalized Born/Solvent Accessibility continuum solvent models. *J Phys Chem B* 2002;106:8726–8738.
  103. Mallik B, Masunov A, Lazaridis T. Distance and exposure dependent effective dielectric function. *J Comp Chem* 2002;23:1090–1099.
  104. Thorgeirsson TE, Russell CJ, King DS, Shin Y-K. Direct determination of the membrane affinities of individual amino acids. *Biochemistry* 1996;35:1803–1809.
  105. Jedlovsky P, Mezei M. Calculation of the free energy profile of H<sub>2</sub>O, O<sub>2</sub>, CO, CO<sub>2</sub>, NO, and CHCL<sub>3</sub> in a lipid bilayer with a cavity insertion variant of the Widom method. *J Am Chem Soc* 2000;122:5125–5131.
  106. Gambu I, Roux B. Interaction of K<sup>+</sup> with a phospholipid bilayer: a MD study. *J Phys Chem B* 1997;101:6066–6072.
  107. Warshel A, Papazyan A. Electrostatic effects in macromolecules: fundamental concepts and practical modeling. *Curr Opin Struct Biol* 1998;8:211–217.
  108. Ben-Tal N, Honig B, Peitzsch RM, Denisov G, McLaughlin S. Binding of small basic peptides to membranes containing acidic lipids. *Biophys J* 1996;71:561–575.
  109. Torres J, Briggs JAG, Arkin IT. Contribution of energy values to the analysis of global searching MD simulations of transmembrane helix bundles. *Biophys J* 2002;82:3063–3071.
  110. Brooks BR, Brucoleri RE, Olafson BD, States DJ, Swaminathan S, Karplus M. CHARMM: a program for macromolecular energy minimization and dynamics calculations. *J Comput Chem* 1983;4:187–217.
  111. Pebay-Peyroula E, Rummel G, Rosenbusch JP, Landau EM. X-ray structure of bacteriorhodopsin at 2.5 Å from microcrystals grown in lipidic cubic phases. *Science* 1997;277:1676–1680.

### APPENDIX: COMPUTATIONAL DETAILS

All computations were performed with the program CHARMM,<sup>110</sup> version c30a1, modified to incorporate the membrane-modeling functionalities. All energy minimizations involved 300 steps of ABNR. All MD simulations were preceded by energy minimization and were performed at 300 K (with rescaling of velocities if necessary) with SHAKE for the bonds involving hydrogen, the Verlet algorithm, and a 2-fs timestep. HBUILD was used to build coordinates for the hydrogen atoms in PDB files. The membrane parameters were  $T = 26 \text{ \AA}$  (unless otherwise noted) and  $n = 10$  (Eq. 7). The following modifications to the EEF1 function were used: the partial charges of Asp, Glu, Arg, and Lys were reduced to better match potential of mean force results in explicit solvent.<sup>61</sup> Corresponding changes were made to the C- and N-terminus. The partial charges of hydroxyl in Ser, Thr, Tyr, and the amide in Gln and Asn were also slightly reduced because they resulted in too strong interactions in water. The modified function is referred to as EEF1.1 (to be published). Helix tilt and crossing angles were determined by using the COOR HELIX command in CHARMM.

Poisson–Boltzmann calculations were performed with the PBEQ module of CHARMM using the extended atom parameters (param19), zero ionic strength,  $0.5 \text{ \AA}$  grid size,  $\epsilon = 1$  for the solute, 80 for water, and either 1 or 2 for the membrane. The nonpolar contribution (SA) was calculated as  $0.033 \text{ kcal/mol \AA}^2 \times$  accessible surface area of the peptide that is within  $\pm T/2$ .<sup>8</sup> The latter was calculated by using the Lee and Richards algorithm and probe radius  $1.4 \text{ \AA}$ .

The coordinates of melittin were obtained from the crystal structure, pdb code 2mlt. The initial transbilayer position was obtained by aligning the principal axis with the bilayer normal. The initial position at the interface was obtained from the Roux lab web page (<http://thallium.med.cornell.edu/RouxLab>). The C-helix of bacteriorhodopsin was built as an ideal helix and placed either perpendicular or parallel to the bilayer with the Asp residues pointing outward. The bacteriorhodopsin simulations started from the crystal structure, pdb code 1ap9.<sup>111</sup> The protein was placed with its principal axis parallel to the bilayer normal and its center of mass at the origin, energy minimized in the membrane, and MD simulated for 200 ps.